







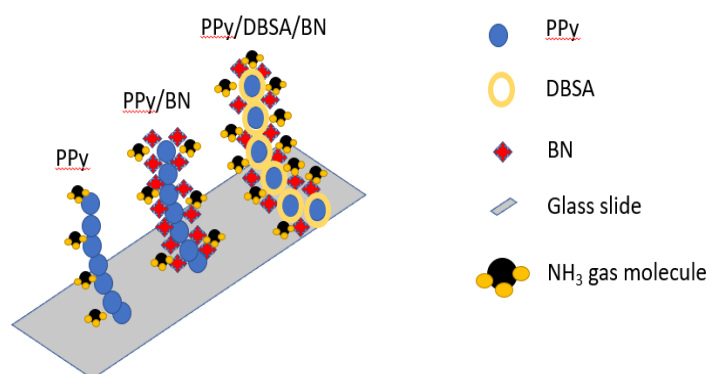
Full Paper | <http://dx.doi.org/10.17807/orbital.v15i3.17875>

Synthesis and Application of Polypyrrole/DBSA/Boron Nitride Ternary Composite as a Potential Chemical Sensor for Ammonia Gas Detection

Kavirajaa Pandian Sambasevam ^{a,b}, Nur Farahin Suhaimi ^a, Izyan Najwa Mohd Norsham ^a, Syed Shahabuddin ^c, Muggundha Raoov ^d, and Siti Nor Atika Baharin* ^a

The present study demonstrates the self-assembly method of chemical oxidative polymerization of polypyrrole (PPy), polypyrrole/boron nitride (PPy/BN), and polypyrrole/dodecylbenzene sulfonic acid/boron nitride (PPy/DBSA/BN) thin films for ammonia (NH₃) gas detection. The PPy, PPy/BN, and PPy/DBSA/BN thin films were comprehensively characterized using Attenuated Total Reflectance Fourier-Transform Infrared Spectroscopy (ATR-FTIR), Scanning Electron Microscopy (SEM), X-ray diffractometry (XRD) and conductivity measurement. ATR-FTIR revealed all the pertinent peaks of PPy, BN, and DBSA present in the PPy/DBSA/BN. SEM images of PPy/DBSA/BN depict well-organized morphology. PPy/DBSA/BN recorded the highest conductivity of $4.771 \times 10^{-6} \text{ S cm}^{-1}$ among the prepared polymer thin films. The obtained characterization results are in good agreement with the NH₃ gas sensor measurements conducted on the PPy/DBSA/BN composite. The linear correlation coefficient between the two was found to be $R^2 = 0.9916$, indicating a strong relationship. Furthermore, the PPy/DBSA/BN thin film demonstrated a low limit of detection (LOD) of 5.8 ppm, surpassing the OSHA threshold value for NH₃ gas. This suggests that the sensor is highly sensitive to trace amounts of NH₃ gas. Moreover, the PPy/DBSA/BN thin film exhibited exceptional reusability, with the ability to be used for up to 10 cycles without a significant decrease in performance. The sensor also demonstrated selectivity towards NH₃ gas in the presence of common interfering species. Additionally, it exhibited long-term stability, maintaining its performance over a period of 7 days. The proposed self-assembled gas sensor has showcased remarkable performance in detecting NH₃ gas at room temperature, making it a promising candidate for industrial applications.

Graphical abstract



Keywords

BN
Gas sensor
PPy
Self-assembly
Semiconductor

Article history

Received 13 Jan 2023
Revised 23 Jun 2023
Accepted 11 Sep 2023
Available online 07 Oct 2023

Handling Editor: Adilson Beatriz

^a Advanced Materials for Environmental Remediation (AMER) Research Group, Faculty of Applied Sciences, Universiti Teknologi MARA, Cawangan Negeri Sembilan, Kampus Kuala Pilah, 72000, Negeri Sembilan, Malaysia. ^b Electrochemical Material and Sensor (EMaS) Group, Universiti Teknologi MARA, Shah Alam, 40450 Selangor, Malaysia. ^c Department of Chemistry, School of Technology, Pandit Deendayal Energy University, Knowledge Corridor, Gandhinagar, Gujarat, India. ^d Department of Chemistry, Faculty of Science, Universiti Malaya, Kuala Lumpur, Malaysia. Corresponding author. E-mail: atikabaharin@uitm.edu.my

1. Introduction

In recent years, the release of excessive toxic air pollutants into the atmosphere from various industrial processes and household activities has become a major source of environmental pollution. Toxic gases such as hydrogen sulfide (H_2S), ammonia (NH_3), and volatile organic compounds (VOC) can cause serious environmental problems that can harm humans and also on other organisms [1]. Among the gases, NH_3 is a common gas in everyday life that may be found in agricultural fertilizers, chemical systems, food processing, and animal husbandry [2–4]. It's also one of the damaging pollutants released into the environment throughout the manufacturing process. NH_3 can cause substantial damage to the eyes, skin, and respiratory system when concentration surpasses 300 ppm [5], representing a major hazard to human health [6]. Occupational Safety and Health Administration's (OSHA) reported that, when the concentration of NH_3 in the workplace surpasses the limits of 35 ppm and 25 ppm, the exposure period should not exceed 15 minutes and 8 hours, respectively [7].

Therefore, many attempts have been made to produce effective NH_3 gas sensors as reported in the literature [8,9]. Particular attention has fallen on conducting polymer (CP) based sensors due to their versatility in terms of light in weight, anti-corrosiveness, tunable electrical and optical properties [10,11]. Among the CPs, polypyrrole (PPy) has shown excellent properties in numerous applications such as gas sensors [12], antibacterial activity, and adsorption reactions [13]. Typically, PPy is one of the most interesting conducting polymers because of its intrinsic electrical conductivity, thermal and environmental durability, biocompatibility, redox characteristics, large surface area, suitability for application in neutral pH regions, and ease of manufacture [14]. Yavarinasab and co-worker have developed PPy based impedimetric sensor for simultaneous detection of H_2S and NH_3 . The sensor exhibited excellent selectivity while distinguishing the signal between H_2S and NH_3 [12]. In another work by Zhang and colleagues have prepared nanofilm of PPy/ Zn_2SnO_4 by self-assembly technique. The sensor was tested at very low concentration of NH_3 gas which ranges from 0.1 – 1.0 ppm and it recorded sub-ppm level detection limit of 0.1 ppm [5]. However, in most cases, PPy is a solid material that is insoluble in organic solvents and infusible at processing temperatures, limiting its processing and potential applications [15]. As a result, many researchers have incorporated inorganic substances into the organic framework of PPy to enhance the key building blocks of organic/inorganic hybrid compounds.

Boron nitride (BN) which is also known as “white graphite” is an inorganic compound that consists of $(\text{BN})_3$ as a layered structure. Although BN is isoelectronic with graphites, due to the covalent inter-bonding between Boron and Nitrogen, it appears to be an insulator in nature. However, BN has drawn a wide range of attention due to its hardness, high-temperature stability, high corrosion resistance, and chemical inertness that could be utilized in a wide spectrum of applications [16,17]. BN can be incorporated with PPy as it may provide a large surface area that enhances signals when the gas molecules penetrate the hybrid PPy/BN and allows more reactive sites for gas sensing [18].

However, the main drawback of organic/inorganic (PPy/BN) hybrid composite is poor catalytic reactions and stability, due to its agglomeration of inorganic compounds [19]. Thus, it would be an advantage to prepare a defect-free

and uniform PPy composite to ensure a better adsorption/diffusion of gas molecules such as NH_3 into the polymer matrix. Dodecylbenzenesulfonic acid (DBSA) is an anionic surfactant and dopant to yield a highly stable colloidal of PPy dispersion [20]. Besides that, the presence of DBSA in the PPy matrix would enhance electron delocalization which will boost the conductivity of resulting PPy composites. An effective electron delocalization always offers an attractive networking system in the gas sensing mechanism.

In the present study, pristine PPy, PPy/BN, and PPy/DBSA/BN composites were prepared via the self-assembly method (SAM). SAM possesses the advantage of producing a thin film that can be directly applied in gas sensor measurement without cumbersome dissolution and coating methods. The synthesized thin films were characterized and effectively applied in NH_3 gas detection. So far as we are concerned, this is the first report on PPy/BN/DBSA composite that was prepared via SAM for gas sensing measurement.

2. Results and Discussion

2.1 ATR-FTIR analysis

Figure 1 shows the FT-IR spectra of BN, pristine PPy, PPy/BN, and PPy/DBSA/BN composites. BN exhibits significant peaks at 1354.58 cm^{-1} (s) and 762.00 cm^{-1} (s) that correspond to the in-plane stretching of B-N and B-N-B bending vibration, respectively [21]. The peaks at 772.00 cm^{-1} (m) and 898.22 cm^{-1} (m) in pristine PPy show the presence of C-H at the pyrrole ring and C=N+-C stretching, respectively. The C=N+-C stretching indicates the polaron characteristics of PPy and suggests that PPy is present in the oxidized state and contains positively charged N^+ moieties. The other peaks of PPy such as 1371 cm^{-1} (s) and 1545 cm^{-1} (m) attributed to C-N stretching and C=C stretching from pyrrole ring moieties, respectively [21]. In comparison to the FTIR spectra of PPy/BN and PPy/DBSA/BN, several peaks showed significant shifts and changes in the intensities. For instance, the strong intensity peaks of B-N and C-N from PPy has overlapped and the intensity decreased at 1371 cm^{-1} (m), meanwhile the B-N-B bending vibration peaks overlapped with C-H stretching of PPy and appeared at 761.15 cm^{-1} (m) and 783.31 cm^{-1} (m) for PPy/BN and PPy/DBSA/BN, respectively. Similarly, the C=N+-C stretching shifted to higher wavenumber $761 - 783\text{ cm}^{-1}$ for the PPy composites. This phenomenon is probably due to the interaction of amide N from the pyrrole ring with the BN particles. Additionally, a new very weak (vw) peak was spotted for PPy/DBSA/BN at 1705 cm^{-1} which corresponds to the C=O stretching that arose from the anionic surfactant, DBSA [13]. These significant shifts and intensity changes clearly show hybrid interaction between PPy, BN and the DBSA and it has been supported by several studies [22,23]. It is the degree of oxidation and length of the conjugated chain that influences the doping level of the PPy which in turn affects the ratio of maximum transmittance [24].

2.2 Scanning electron microscopy (SEM) analysis

Figure 2 represents SEM images of (a) BN, (b) pristine PPy, (c) PPy/BN and (d) PPy/DBSA/BN. The BN SEM image was recorded at a high magnification of 30000 \times , to showcase their nano-scale size. Pristine PPy resembles a porous surface with the agglomeration of tiny globules due to the formation of aggregates, which results in a uniform surface morphology known as “cauliflower” in Figure 2 (b) [24]. The surface

morphology of PPy/BN in Figure 2(c), reveals the alteration of the flake-like structures into a more porous polymeric network. The addition of BN nanosheets does not alter the surface morphology of PPy polymer but the surface has been modified into much porous as depicted in the SEM image. The BN nanosheets can be seen on the PPy surface (marked by red arrows and yellow circles) embedded deep within the polymeric network. Hence, it can be stated that BN nanosheets possess a nucleating effect on the pyrrole polymerization and cause a homogeneous PPy shell around them. Thus, the morphological analysis reveals the formation of flakes like PPy and BN doped PPy composite and no free BN nanosheets were present [25]. Figure 2 (d) shows the morphology of PPy/ DBSA/BN, that incorporated with anionic surfactant (DBSA) and thus, BN has expanded the PPy formation, thereby allowing the organic solvent to diffuse into the spaces between the PPy backbones that lead to a large globular structure of PPy that consists of sticky property of DBSA [26].

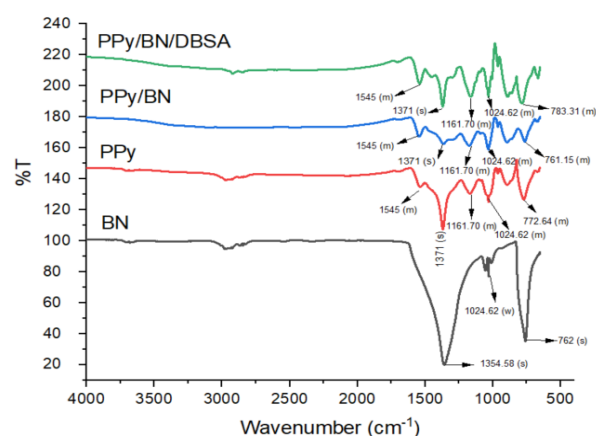


Fig. 1. FTIR spectra of BN, PPy, PPy/BN, PPy/DBSA/BN. [Abbreviations for the intensities: strong (s), medium (m), weak (w), and very weak (vw)].

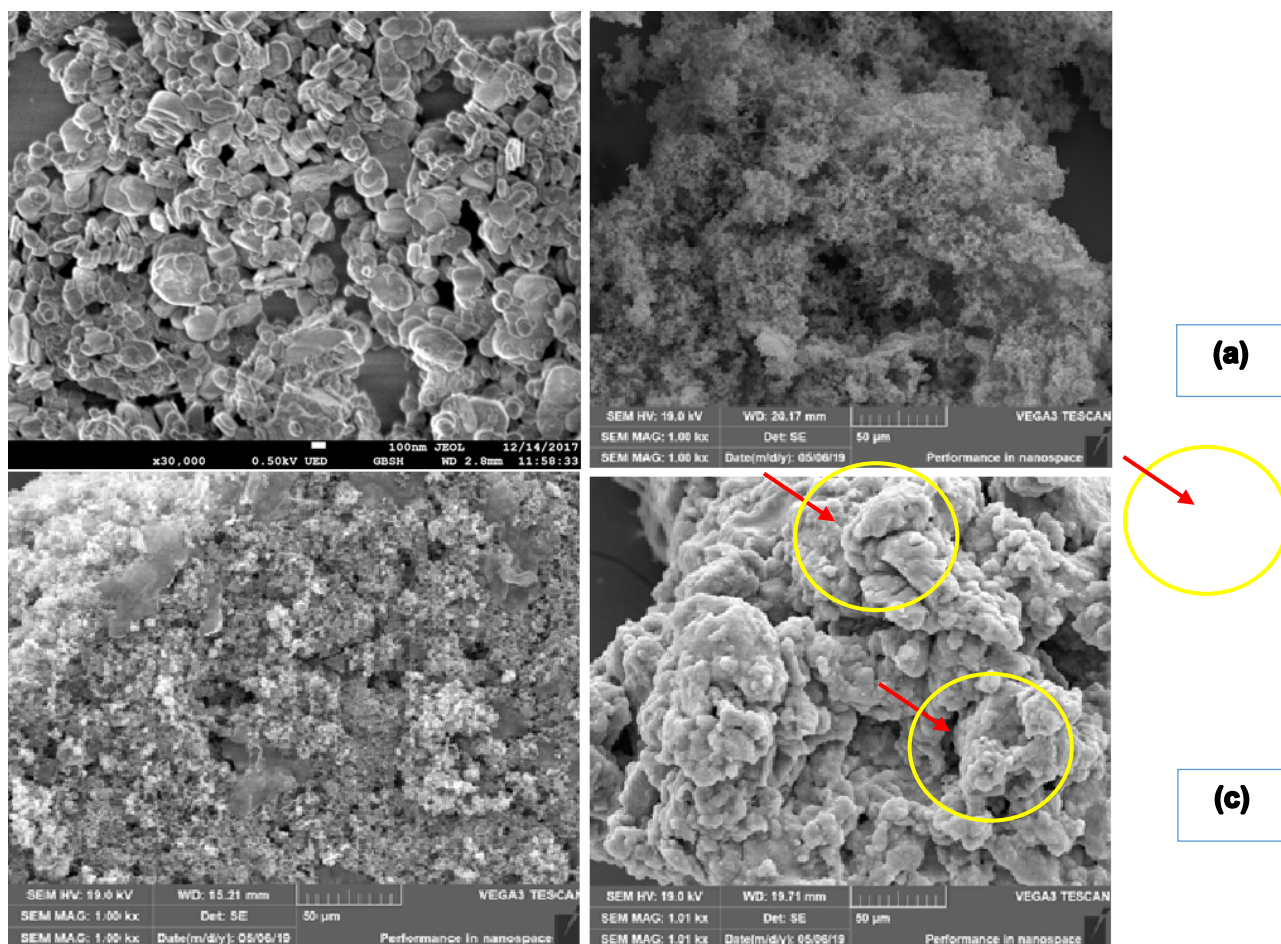


Fig. 2. SEM morphology for (a) BN (b) PPy (c) PPy/BN and (d) PPy/DBSA/BN.

2.3 X-ray diffractometer (XRD) analysis

Figure 3 shows the XRD peaks of BN, pristine PPy, PPy/BN, and PPy/DBSA/BN. BN shows crystalline peaks at $2\theta = 26.68^\circ$, 41.52° , 49.76° , 54.96° , and 75.52° which are similar to the previously reported studies [16,21,27]. Pristine PPy exhibits an amorphous nature in the X-ray diffractograms. Typically, it shows an infused broad peak at $2\theta = 19.64^\circ$ and 26.71° that corresponds to the scattering of PPy chains at the interplanar

spacing [12,28]. PPy/BN exhibits four peaks at $2\theta = 26.68^\circ$, 41.52° , 54.96° , and 75.52° where the diffractogram mainly depicts the crystalline nature of BN. The well-defined and intense peak at 26.68° corresponds to the (002) structure of BN [21]. However, the significant amorphous peak of PPy is not seen in the diffractogram, which shows the presence of predominance BN crystallites. PPy/DBSA/BN records several peaks that overlap with the PPy and BN peaks. Ironically, the amorphous peak of PPy at $2\theta = 20.48^\circ$ is more obviously

recorded with a slight shift. Probably, the presence of bulky anionic surfactant retains and enhanced PPy characteristics in the ternary composite which also could be the reason for the diminishing intensity of prominent BN peak at $2\theta = 26.71$. The inset in Figure 3 depicts the respective crystallinity index (CI) of the samples. The CI is well supported by the amorphous and crystalline nature of the samples. BN reported the highest CI of 61.96% due to its crystalline nature. The

remaining PPy composites follows an order PPy/DBSA/BN > PPy/BN > PPy with CI = 42.03, 29.43, 23.20, respectively. This phenomenon is well aligned with the SEM images of samples, where among the composites – PPy/DBSA/BN resembles a closely packed structure due to the presence of BN nanosheets. This order of arrangement will increase the CI of the material [29].

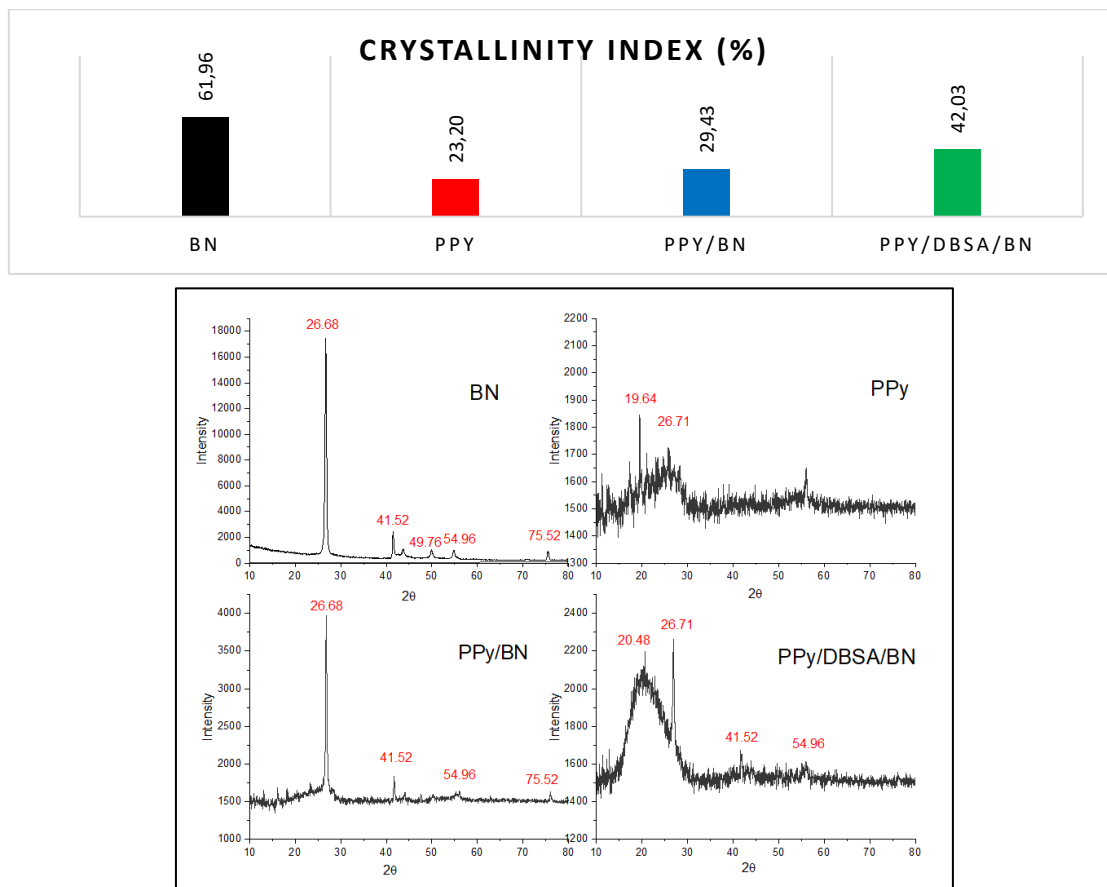


Fig. 3. X-ray diffractograms of BN, PPy, PPy/BN, and PPy/DBSA/BN. The inset at the top shows the crystallinity index of the respective material.

2.4 Conductivity PPy and PPy composite thin films

PPy, PPy/BN, and PPy/DBSA/BN thin films exhibited conductivities such as $2.143 \times 10^{-7} \text{ S cm}^{-1}$, $3.965 \times 10^{-6} \text{ S cm}^{-1}$, and $4.771 \times 10^{-6} \text{ S cm}^{-1}$, respectively. The conductivity of PPy is the lowest due to the presence of a long alkyl chain on the pyrrole ring that causes a steric hindrance that affects the planarity of the resulting polymer. The PPy/BN thin film's electrical conductivity is influenced by the presence of semiconductor, BN on the backbone of PPy. The semiconductor added electrons to the PPy backbone while withdrawing electrons from PPy. The addition of BN causes the electron to excite from the highest occupied molecular orbital (HOMO) of the valence band (oxidation) to the lowest unoccupied molecular orbital (LUMO) of the conduction band (reduction). These produce charge carriers in the polymer in the form of polarons (radical ions), bipolarons (dications or dianions), or solitons. Solitons serve as the charge carriers along the polymer chains that enhance the conductivity [30]. Among the films, PPy/DBSA/BN composite recorded a higher conductivity than PPy and PPy/BN, due to the addition of DBSA and BN into the PPy/DBSA/BN molecular structure as it results in higher crystallinity which facilitates the charge transfer mechanism and hence, increased electrical

conductivity [22,30]. Also, the interaction of DBSA increases the electrical conductivity due to the unlocking of polarons or bipolarons [30,31].

2.5 Sensor Performance of PPy and PPy composite thin films

2.5.1 Calibration Curve

Figure 4 depicts the calibration curves of pristine PPy, PPy/BN, and PPy/DBSA/BN thin films in a linear range of 10 – 50 ppm for NH_3 gas detection. Typically, all thin films exhibited an increased pattern in the % of sensitivity as the concentration of NH_3 gas increased in the gas chamber [32]. Among the PPy and PPy composites, PPy/DBSA/BN exhibited an excellent and the highest correlation of coefficient of $R^2 = 0.9916$ which is close to unity [33]. The calculated limit of detection (LOD) and limit of quantitation (LOQ) for the PPy/DBSA/BN is 5.80 ppm and 17.58 ppm, respectively which is the lowest compared to PPy and PPy/BN. Generally, in the principle of a gas sensor, the gaseous species will move with high kinetic energy and interact with the sensor material [31]. Hence, the active surface area of the sensor material is of paramount interest for efficient analyte gas detection. The presence of bulky anionic surfactant, DBSA in the PPy/BN

formulation has provided a large surface area for the synergistic interaction towards NH_3 gaseous molecules. This phenomenon is well supported by the SEM morphology analysis in Figure 2. Besides that, the high crystallinity of PPy/DBSA/BN (inset of Figure 3) caters to an ordered

structure between the PPy-DBSA-BN which also facilitates the sensor measurement [29]. Therefore, sensor performance analysis such as optimum response time, selectivity, reusability, and long-term stability has been carried out on PPy/BN/DBSA thin film.

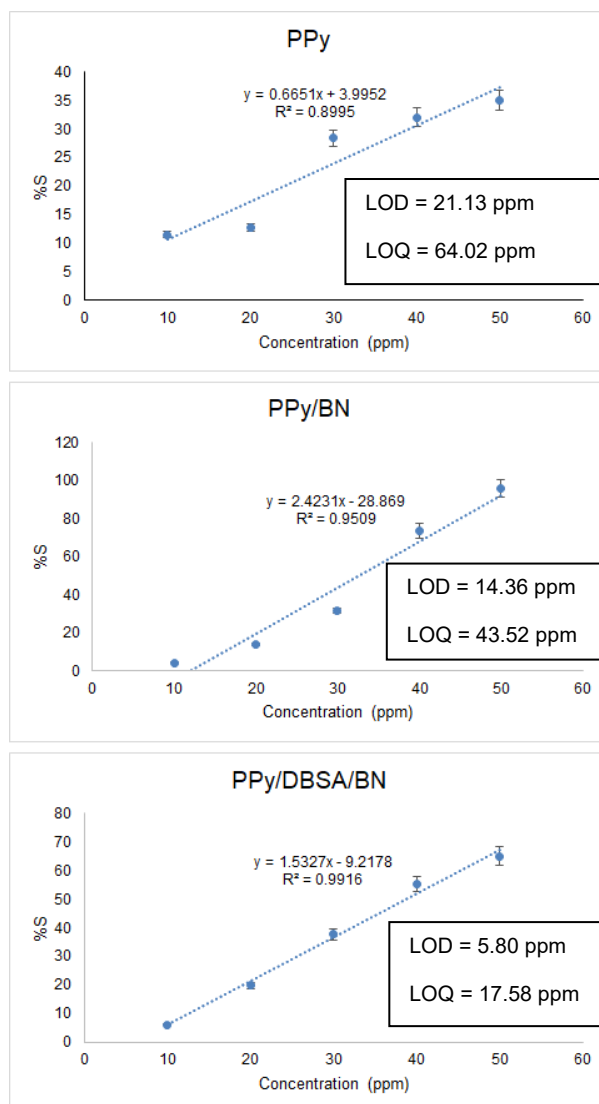


Fig.4. Calibration curves of pristine PPy, PPy/BN, and PPy/DBSA/BN with its respective LOD and LOQ.

2.5.2 Optimum response time

Figure 5 shows the response of PPy/DBSA/BN thin films against a different concentration of NH_3 gas at different response times. Herein, the quality of the thin film in terms of response time was assessed based on the highest linearity factor. In that sense, PPy/DBSA/BN recorded the highest linearity with $y = 1.4583x - 6.2403$ ($R^2 = 0.9884$) at 5 min response time. In addition, the PPy/DBSA/BN reported the highest sensor sensitivity of 1.4583 ppm^{-1} based on its value from the slope [37]. Therefore, a response time of 5 mins was selected as the stable optimum time for NH_3 gas detection by PPy/DBSA/BN.

It is always essential to compare the performance of the sensor from this study with other reported sensors in the literature to get an overview. Hence, Table 1 reports various sensors with their respective linear range, LOD, instrumentation, and methods that were used to detect the

gaseous NH_3 . For comparison purposes, different types of materials were selected including metal oxide [38], polyaniline (PANI) [39], metal-doped PPy [40,41], and PANI doped with dioctyl sulfosuccinate sodium [42]. The researchers from the respective studies have used expensive and cumbersome setups in their sensor measurements. In addition, pure metal-based fillers also can boost the construction cost of the sensors. Generally, PPy/DBSA/BN exhibited the lowest limit of detection (5.8 ppm) compared to the selected sensors in the NH_3 gas detection. Moreover, the threshold value of NH_3 gas detection is less than 25 ppm [40]. Therefore, PPy/DBSA/BN is an excellent candidate for gaseous NH_3 detection.

2.5.3 Selectivity study

The selectivity study was done by exposing the PPy/DBSA/BN thin film to different types of gases such as NH_3 , acetone (CH_3COCH_3), methanol (CH_3OH), and hexane (C_6H_{14}) at a similar concentration of 10 ppm at 50°C .

PPy/DBSA/BN thin film showed high selectivity towards NH_3 gas as shown in Figure 6. It reveals that high molecular weight compounds like alcohols and alkanes are unable to penetrate polymer matrix as efficiently as small molecules due to their long-chain lengths and non-polar character, the composite film was not highly selective on them. As a result, it will increase the resistance, as they are likely to act as barriers to PPy/DBSA/BN backbone. Therefore, acetone was not very selective as it can weaken the dispersion force between aromatic Py units, which hinders the electron mobility of PPy/DBSA/BN [43]. The film exhibits a high response toward NH_3 gas due to the presence of sulfonyl groups of DBSA that generates electrostatic interaction with NH_3 gas [44]. Meanwhile, the interaction of electron-deficient nitrogen and negatively charged boron atoms of the BN ring causes an increase in the mobility of charge carriers thereby increasing the sensing behavior of PPy/DBSA/BN thin film. Sensing behavior depends on the intensity of interaction between the target gas and the sensing layer [43].

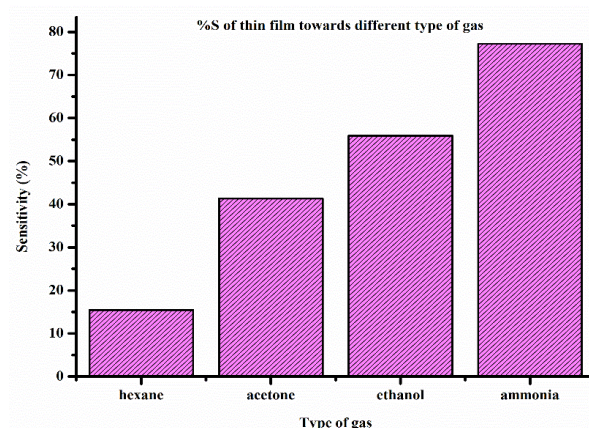


Fig. 6. Selectivity of PPy/DBSA/BN against different types of gases.

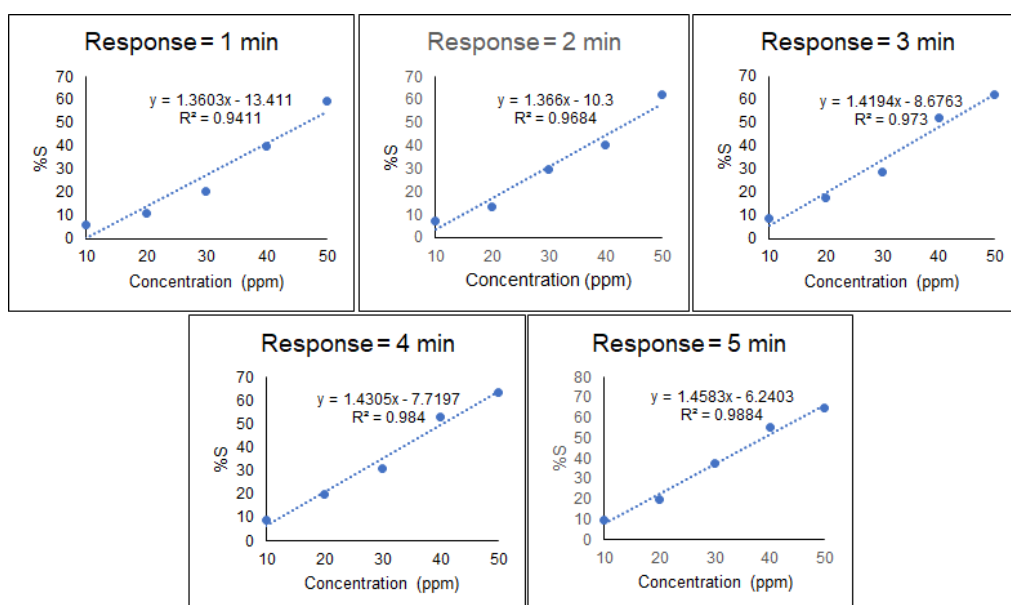


Fig. 5. Sensor response of PPy/DBSA/BN at different time intervals against the different concentrations of NH_3 gas.

Table 1. Comparison of various sensor materials in NH_3 gas detection.

Sensor Material	Linear range (ppm)	Lowest detected concentration (ppm)	Instrument	Method	Ref
ZnO/Pd	30 – 300	30	Kinesistec testing station	Resistance	[38]
PANI/ZnO	25 – 100	25	Potentiometric	Resistance	[39]
Pt doped PPy	10 – 50	10	Surface acoustic wave	Frequency	[40]
PPy-Ag	50 – 500	50	Scientific Programmable Digital Multimeter	Resistance	[41]
PANI/AOT	40-100	11	Multimeter	Resistance	[42]
PPy/DBSA/BN	10 – 50	5.80	Multimeter	Resistance	This work

2.5.4 Reusability study

PPy/DBSA/BN thin films have shown some promising results toward NH_3 gas detection. Reusability depicts how many times a thin film can be reused till it gets exhausted. Typically, the ability of the film as a sensor to keep up its performance for several cycles is one of the important keys to a versatile sensor. To serve this purpose, PPy/DBSA/BN thin film was subjected to dynamic NH_3 (ON) and HCl (OFF) gases

alternatively in Figure 7. The thin film was dedoped by NH_3 and redoped by HCl gases for 10 repeated cycles. The results show that the sensor resistance increases upon exposure to NH_3 and then decreases when redoped with HCl in all the sequential experiments. The decrease in resistance when introduced to HCl shows almost complete removal of adsorbed NH_3 molecules from the sensor surface. This shows that the NH_3 molecules and sensing surface possess a weak

attraction of forces as a result, the adsorbed molecules are easily detached by the kinetic energy of the HCl [45]. Thus, from the graph, it can be concluded that the thin films show good reusability up to 10 cycles in continuous measurements due to the addition of BN which stabilizes the PPy.

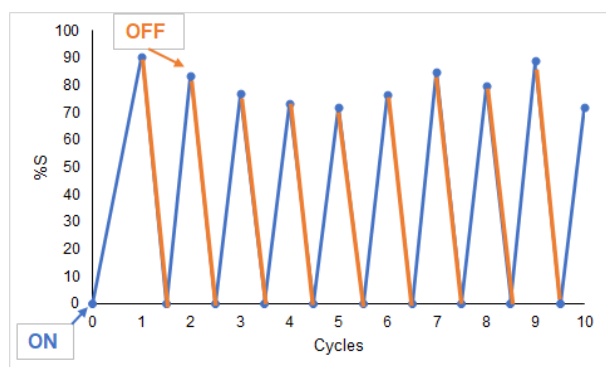


Fig. 7. Reusability of PPy/DBSA/BN thin film in NH_3 gas detection for continuous 10 cycles.

2.5.5 Long-term stability study

Figure 8 shows the long-term stability of PPy/DBSA/BN thin film in 10 ppm of NH_3 gas detection for up to 7 days. After each dedoping (by NH_3) / redoping (by HCl), the PPy/DBSA/BN thin film was kept inside the fume hood at ambient temperature. Overall, the thin film exhibited a decreased trend in the response stability which is a common

3.1 Materials

Pyrrole (Py) monomer (99%), boron nitride (BN), and dodecylbenzene sulfonic acid (DBSA) were purchased from Sigma Aldrich (Malaysia). Ammonium persulfate (APS) was purchased from R&M (Malaysia) and distilled water was used throughout the experiments.

3.2 Synthesis of pristine PPy and PPy composite thin films via a self-assembly method

Self-assembled thin films are great for gas sensor measurements due to their uniform nature during the formation of polymer composite structures [44]. Therefore, the pristine PPy and PPy composites were synthesized via the self-assembly technique for the gas sensor application. Hence, thin films of the polymer composites were made via the self-assembly method on a microscope glass slide. The glass substrates underwent pre-treatment using concentrated HNO_3 in order to generate radicals capable of bonding with Py monomers.

3.3 PPy thin film

Typically, Py suspension of 5 mmol was dispersed in distilled water and stirred for 30 minutes. Next, 10 μL of this suspension was dropped on a pre-treated glass substrate. After that, 10 μL of 5 mmol of APS (dissolved in 1M HCl) was dropped on the Py droplet. Then, the mixtures were left to polymerize for 4 hours. Subsequently, the dried PPy film was washed with distilled water several times and dried at ambient temperature.

3.4 PPy/BN thin film

Before the PPy/BN preparation, 1 mmol of BN was prepared under sonication for 1 hour. Separately, Py

characteristic of the sensor if placed in an ambient environment [8]. Typically, PPy/DBSA/BN showed a drastic decrease in sensitivity up to Day 3. Then, the response stabilized till Day 7 before it loses major sensitivity in the subsequent days due to the influence of humidity. This may deteriorate the available active sites of thin-film, that's responsible for the sensing mechanism. Thus, it can be concluded that PPy/DBSA/BN thin film is good to use for 7 days in NH_3 gas detection [42].

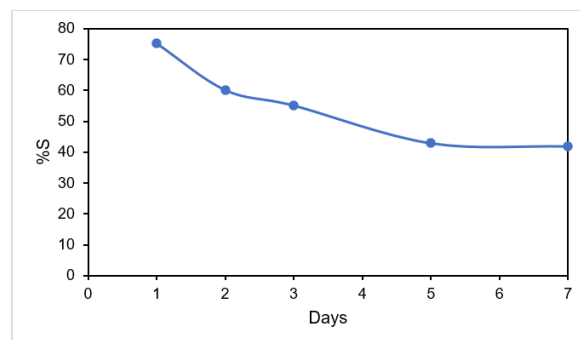


Fig. 8. Long-term stability of PPy/DBSA/BN thin film against 10 ppm of NH_3 gas.

3. Material and Methods

suspension of 5 mmol in distilled water was dropped on the pre-treated glass substrate followed by the addition of 10 μL of BN suspension. After that, 10 μL of 5 mmol of APS solution was dropped on the Py/BN droplet. Later, the composite film was let to polymerize for 4 hours and then washed with distilled water repeatedly. Finally, the prepared thin film of PPy/BN was dried at ambient temperature.

3.5 PPy/DBSA/BN thin film

BN suspension of 1 mmol in distilled water was added to an equimolar ratio of Py/DBSA milky suspension and stirred for 30 minutes. Then, 10 μL of Py/DBSA/BN suspension was dropped on a pre-treated glass substrate. Next, 10 μL of 5 mmol APS solution was dropped on the Py/DBSA/BN droplet and let polymerize for 4 hours. After the polymerization, the thin film was washed and dried at ambient temperature. The resulting film was labeled as PPy/DBSA/BN.

3.6 Characterizations

The BN, pristine PPy, and PPy composites were characterized by attenuated total reflectance-Fourier transform infrared (ATR-FTIR) Perkin Elmer model 100 spectrometer in the range of 4000 – 650 cm^{-1} . The thin films were scratched and placed at the ATR probe prior to the FTIR analysis. Scanning Electron Microscope (SEM), model TESCAN VEGA3 was used to study the morphology of BN, pristine PPy, and PPy composites. The samples were undergone platinum sputtering of 1 nm thickness prior to SEM analysis. A secondary electron detector was used throughout the morphology analysis. X-ray diffractograms were recorded by an Empyrean X-ray diffractometer (XRD) equipped with Cu K α radiations ($\lambda = 1.5418 \text{ \AA}$) at a scan rate of 0.02 sec^{-1} in the 2θ range of 10° to 80°. The resistance of pristine PPy and PPy composites was recorded using a digital multimeter (Fluke,

15B Digital Multimeter) using a two-point probe method. Then, the resistance was employed in equation (1) to calculate the surface conductivity (σ) of the samples.

$$\sigma = \frac{\text{Distance between two probes (cm)}}{\text{Resistance } (\Omega) \times \text{Area of the film (cm}^2\text{)}} \quad (1)$$

3.7 Gas Sensor Measurement

The performance of pristine PPy and PPy composites in NH_3 gas sensing was recorded in a dynamic concentration range of 10 – 50 ppm. The resistance of the samples was recorded during the detection process and recalculated using equation (2) for the % of sensitivity (%S).

$$\%S = \left| \frac{(R_f - R_i)}{R_i} \right| \times 100 \quad)$$

where R_i = initial resistance and R_f = final resistance. The resistance was measured by using a digital multimeter (Fluke). The %S was used to construct the calibration curve and the limit of detection (LOD), the limit of quantitation (LOQ), and correlation coefficients (R^2) were calculated and tabulated for comparison purposes according to equations (3) and (4) [45]. Among the polymers, PPy/DBSA/BN exhibited the highest R^2 and lowest limit of detection, hence, it was chosen to study the sensor performances (selectivity, reusability, and long-term stability) in NH_3 gas detection.

$$\text{LOD} = \frac{3.3 \text{ STEYX}}{\text{slope}} \quad (3)$$

$$\text{LOQ} = \frac{10 \text{ STEYX}}{\text{slope}} \quad (4)$$

4. Conclusions

In conclusion, PPy/DBSA/BN was successfully synthesized via chemical oxidative polymerization by employing the self-assembly technique. Characterizations such as FTIR, SEM, and XRD confirmed the chemical interactions between the PPy, DBSA, and BN components. The presence of BN in the PPy/DBSA matrix improved the crystallinity and enhanced the conducting properties. Therefore, the mobility of electrons within the PPy/DBSA/BN matrix enhanced the NH_3 gas detection mechanism as well. This study reported a LOD of 5.8 ppm which is lower than the threshold value set for gaseous NH_3 exposure. In addition, PPy/DBSA/BN recorded a good selectivity, reusability, and long-term stability that is sufficient for a gas sensor. The use of a maintenance-free multimeter will reduce the total cost of NH_3 gas detection. Hence, the PPy/DBSA/BN thin films provide an alternative material for NH_3 gas detection with cheap labor costs for environmental monitoring.

Acknowledgments

The authors wish to thank Research Centre for Nano-Materials and Energy Technology, Sunway University, Malaysia for allowing us to perform Scanning Electron Microscopy (SEM) at their facility. No financial support was received for this project.

Author Contributions

Kavirajaa Pandian Sambasevam: Conceptualization, Data Curation, Software, Supervision, Validation, & Writing – review & editing. Nur Farahin Suhaimi: Formal analysis, Investigation, Writing – original draft. Izyan Najwa Mohd Norsham: Formal analysis, Syed Shahabuddin: Writing – review & editing, Muggundha Raoov: Methodology, Writing – review & editing, and Siti Nor Atika Baharin: Supervision, Writing – review & editing.

References and Notes

- [1] Dunst, K. J.; Cysewska, K.; Kalinowski, P.; Jasiński, P. *IOP. Conf. Ser. Mater. Sci. Eng.* **2016**, 12, 18. [\[Crossref\]](#)
- [2] Gençer, E.; Burniske, G. R.; Doering, O. C.; Tyner, W. E.; Agrawal, R.; Delgass W. N. *Biofuels, Bioprod. Biorefining.* **2020**, 14, 725. [\[Crossref\]](#)
- [3] Zhang, Q.; Guo, N.; Chen, Y.; Fu, Y.; Zhao, Q. *Micromachines* **2019**, 10, 573. [\[Crossref\]](#)
- [4] Lee, C. T.; Wang, Y. S. *J. Alloys. Compd.* **2019**, 789, 693. [\[Crossref\]](#)
- [5] Zhang, D.; Wu, Z.; Zong, X.; Zhang, Y. *Sensors Actuators, B. Chem.* **2018**, 274, 575. [\[Crossref\]](#)
- [6] He, J.; Yan, X.; Liu, A.; You, R.; Liu, F.; Li, S. *J. Mater. Chem. A.* **2019**, 7, 4744. [\[Crossref\]](#)
- [7] Li, S.; Liu, A.; Yang, Z.; Zhao, L.; Wang, J.; Liu, F. *Sensors Actuators, B. Chem.* **2019**, 289, 252. [\[Crossref\]](#)
- [8] Mazlan, N. A.; Sapari, J. M.; Sambasevam, K. P. *J. Met. Mater. Miner.* **2020**, 30, 50. [\[Link\]](#)
- [9] Indarit, N.; Kim, Y.; Petchsang, N.; Jaisutti, R. *RSC Adv.* **2019**, 9, 26. [\[Crossref\]](#)
- [10] Farea, M. A.; Mohammed, H. Y.; Shirsat, S. M.; Sayyad, P. W.; Ingle, N. N.; Al-Gahouari T. *Chem. Phys. Lett.* **2021**, 776, 138. [\[Crossref\]](#)
- [11] Moshayedi, H. R.; Rabiee, M. *J. Chem. Chem. Eng.* **2020**, 39, 93. [\[Crossref\]](#)
- [12] Yavarinasab, A.; Janfaza, S.; Tahmooressi, H.; Ghazi, M.; Tasnim, N.; Hoorfar, M. *J Hazard. Mater.* **2021**, 416, 125. [\[Crossref\]](#)
- [13] Sambasevam, K. P.; Mohamad, S.; Phang, S. W. *Malaysian J. Anal. Sci.* **2017**, 21, 762. [\[Crossref\]](#)
- [14] Shahabuddin, S.; Mazlan, N. A.; Baharin, S. N. A.; Sambasevam, K. P. *Engineering Materials* **2021**, 1. [\[Crossref\]](#)
- [15] Balakumar, V.; Prakash, P. *J. Catal.* **2016**, 344, 795. [\[Crossref\]](#)
- [16] Selvarajan, S.; Suganthi, A.; Rajarajan, M. *Ultrason. Sonochem.* **2018**, 44, 319. [\[Crossref\]](#)
- [17] Eichler, J.; Lesniak, C. *J. Eur. Ceram. Soc.* **2008**, 28, 1105. [\[Crossref\]](#)
- [18] Shi, L.; Gu, Y.; Chen, L.; Qian, Y.; Yang, Z.; Ma, J. *J. Solid State. Chem.* **2004**, 177, 721. [\[Crossref\]](#)
- [19] Madakbaş, S.; Sen, F.; Kahraman, M. V.; Dumludag F. *Adv. Polym. Technol.* **2014**, 00, 21438. [\[Crossref\]](#)
- [20] Golabi, M.; Padiolleau, L.; Chen, X.; Jafari, M. J.; Sheikhzadeh, E.; Turner, A. P. F. *PLoS One.* **2016**, 11, e0166548. [\[Crossref\]](#)
- [21] Zanini, B. C.; Santos, L. M.; Romio, A. P.; Domenico, M. D.; Santos, A. F.; Hermes, D. A. P. *H. Mater. Today.*

- Commun.* **2021**, 26, 2352. [\[Crossref\]](#)
- [22] Kee, L. P.; Moozarm, N. P.; Meng, W. P. *Electrochim. Acta* **2017**, 246, 841. [\[Crossref\]](#)
- [23] Sambasevam, K. P.; Mohamad, S.; Phang, S.-W. *Mater. Sci. Semicond. Process.* **2015**, 33, 24. [\[Crossref\]](#)
- [24] Sultan, A.; Mohammad, F. *Polymer* **2017**, 113, 221. [\[Crossref\]](#)
- [25] Sultan, A.; Ahmad, S.; Anwer, T.; Mohammad, F. *RSC. Adv.* **2015**, 5, 105980. [\[Crossref\]](#)
- [26] Shahabuddin, S.; Khanam, R.; Khalid, M.; Saidur, R. *Arab. J. Chem.* **2018**, 11, 1000. [\[Crossref\]](#)
- [27] Sun, W.; Guo, J.; Ou, H.; Zhang, L.; Wang, D.; Ma, Z.; Zhu, B.; Ali, I.; Naz, I. J. *Solid State. Chem.* **2022**, 311, 123073. [\[Crossref\]](#)
- [28] Mettai, B.; Mekki, A.; Merdj. F.; Bekkar, Z.; Sayah, D.; Soumia, K.M. *J. Polym. Res.* **2018**, 95, 25. [\[Crossref\]](#)
- [29] Jayamurgan, P.; Ponnuswamy, V.; Ashokan, S.; Mahalingam, T. *Iran. Polym. J.* **2013**, 22, 219. [\[Crossref\]](#)
- [30] Atar, N.; Yola, M. L. *J. Electrochem. Soc.* **2018**, 165, H255. [\[Crossref\]](#)
- [31] Chougule, M. A.; Pawar, S. G.; Godse, P. R.; Mulik, R. N.; Sen, S.; Patil, V. B. *Soft Nanosci. Lett.* **2011**, 01, 11002. [\[Crossref\]](#)
- [32] Sambasevam, K. P.; Mohamad, S.; Phang, S.-W. *J. Appl. Polym. Sci.* **2015**, 132, 41746. [\[Crossref\]](#)
- [33] Le, T. H.; Kim, Y.; Yoon, H. *Polymers* **2017**, 9, 150. [\[Crossref\]](#)
- [34] Sravanthi, M.; Manjunatha, K. G. *Mater. Today. Proc.* **2021**, 46, 5964. [\[Crossref\]](#)
- [35] Mane, A. T.; Navale, S.T.; Patil, V. B. *Org. Electron.* **2015**, 19, 15. [\[Crossref\]](#)
- [36] Mohd. Norsham I. N.; Baharin, S. N. A.; Raoov, M.; Shahabuddin, S.; Jakmunee. J.; Sambasevam, K. P. *Polym. Eng. Sci.* **2020**, 60, 3170. [\[Crossref\]](#)
- [37] Zhang, L.; Liu, J.; Peng, X.; Cui, Q.; He, D.; Zhao, C. *Synth. Met.* **2020**, 259, 116. [\[Crossref\]](#)
- [38] Mhlongo, G. H.; Motaung, D. E.; Swart, H. C. *Mater. Lett.* **2015**, 160, 200. [\[Crossref\]](#)
- [39] Sambasevam, K. P.; Sateria, S. F.; Baharin, S. N. A.; Azman, N. J.; Wakid, S. A.; Shahabuddin, S. *Int. J. Biol. Macromol.* **2023**, 238, 124079. [\[Crossref\]](#)
- [40] Chen, X.; Li, D.M.; Liang, S.F.; Zhan, S.; Liu, M. *Sensors Actuators B. Chem.* **2013**, 177, 364. [\[Crossref\]](#)
- [41] Nerkar, D. M. S. *Int. J. Res. Appl. Sci. Eng. Technol.* **2018**, 6, 1241. [\[Link\]](#)
- [42] Mustapa, R.; Abu Mansor, Z. I.; Sambasevam, K. P. *J. Phys. Sci.* **2018**, 29, 9. [\[Crossref\]](#)
- [43] Jain, S.; Karmakar, N.; Shah, A.; Kothari, D. C.; Mishra, S.; Shimpi, N. G. *Appl. Surf. Sci.* **2016**, 396, 1317. [\[Crossref\]](#)
- [44] Mane, A. T.; Sartale, S. D.; Patil, V. B. *J. Mater. Sci. Mater. Electron.* **2015**, 26, 8497. [\[Crossref\]](#)
- [45] Khan, I.; Saeed, K.; Khan, I. *Arab. J. Chem.* **2019**, 12, 908. [\[Crossref\]](#)

How to cite this article

Sambasevam, K. P.; Suhaimi, N. F.; Norsham, I. N. M.; Shahabuddin, S.; Raoov, M.; Baharin, S. N. A. *Orbital: Electron. J. Chem.* **2023**, 15, 133. DOI: <http://dx.doi.org/10.17807/orbital.v15i3.17875>